

Exploring functionalized Zr_2N and Sc_2N MXenes as superconducting candidates with *ab initio* calculations

Alpin N. Tatan^{1,2,*} and Osamu Sugino^{1,2}

¹*Department of Physics, Graduate School of Science,
The University of Tokyo, 7-3-1 Hongo, Bunkyo-ku, Tokyo, 113-0033, Japan.*

²*The Institute for Solid State Physics, The University of Tokyo,
5-1-5 Kashiwanoha, Kashiwa, Chiba, 277-8581, Japan.*

(Dated: March 8, 2025)

We explore the possibility of obtaining new superconductor candidates from functionalized MXene compounds Zr_2NS_2 , Zr_2NCl_2 , and Sc_2NCl_2 based on *ab initio* calculations with density functional theory for superconductors (SCDFT). The predicted superconducting transition temperature (T_c) at ambient pressure may reach up to 9.48 K (Zr_2NS_2), while further T_c improvements may be achieved with applied strain. We note a correlation between the profiles of superconducting gap (Δ) and electron-phonon coupling (λ) across the Fermi surface for all compounds, which may be influenced by their modified electronic bandstructure components.

I. INTRODUCTION

MXenes ($M_{n+1}X_n$) are two-dimensional (2D) materials made of two or more layers of transition metal (M) atoms sandwiching carbon or nitrogen (X) layers [1]. MXenes have a hexagonal close-packed (hcp) crystal structure with a $P6_3/mmc$ space group symmetry, where the transition metals in M sites are close-packed, and the X atoms occupy octahedral sites in between the M atomic planes [1]. This family of 2D materials generally has metallic, nonmagnetic structure with quite large density of states at Fermi level [2, 3], opening itself to many potential applications [1, 2].

In its synthesis, MXenes are often obtained with additional surface terminations [2]. The presence of surface functional groups ($T = Cl, S, \dots$) may modify the properties of MXenes. In the case of Nb_2C , functionalization with Cl or S leads to superconductivity [4–10] while the bare, O- or F-terminated compounds do not superconduct at temperatures as low as 2 K [4, 5]. Mixture of surface terminations, e.g., Cl combined with F, O, etc. may also suppress superconductivity [7]. Although the nature of superconductivity in these compounds is unconfirmed, similarities to electron-phonon mechanism based on pressure dependence and specific heat measurements have been noted [6]. *Ab initio* studies [5, 9, 10] based on McMillan formula [11] have also reported comparable transition temperature (T_c) values.

As far as we know, superconductivity in functionalized MXenes remains largely unexplored: the Nb_2C family being the only confirmed system to exhibit this property. Historically, the presence of multiple systems sharing similar phenomena is beneficial for improving their comprehension, as lessons derived from one system may be utilized for others [12]. The interrelated studies of various cuprate and nickelate superconductors exemplify this practice [13–23]. Hence, it is worthwhile to explore

other MXene compounds whose superconductivity may be enabled with surface functionalization. This is the main objective in this paper.

We leverage on past studies [3, 24, 25] to shortlist the vast combinations of MXenes and functional groups to be explored in this paper. We focus on the simplest case of $n = 1$ as this group hosts an experimentally known superconductor (Nb_2CT_2). Among the possible configuration sites in the functionalized MXene M_2XT_2 , the structure depicted in Figure 1 is generally deemed to be most stable [2, 9, 10, 24–26]. We consider functionalization with $T = Cl$ and S , as these are known experimentally to induce superconductivity in Nb_2C [4]. We remark that Nb_2CSe and Nb_2CNH were also reported to superconduct [4], but these cases may involve compounds containing high number of vacancies [9] or with uncertain distribution of the T atoms over the MXenes that make their simulation nontrivial. Hence, we limit our scope only to explore the structures in Figure 1 with $T = Cl$ and S in this paper.

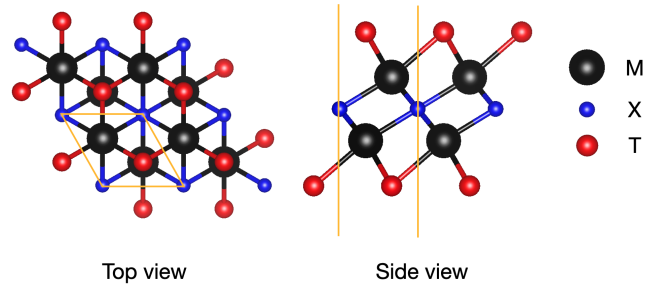


FIG. 1. Top and side views of the crystal structure model for functionalized MXenes M_2XT_2 . Solid orange lines mark the unit cell. Black, blue, and red spheres represent the transition metal atoms M, the C or N atoms X, and the functional group atoms T, respectively.

A prior computational study [3] has screened bare MXenes (M_2X) for potential superconductor candidates. Since our objective is to obtain superconductivity through functionalization, we select the compounds

* alpinnovianustatan@gmail.com

from Ref. [3] which do not superconduct in their bare forms. Subsequently, we combine these with prior stability screenings on functionalized MXenes using Cl and S functional groups [24, 25]. From the stable compounds, we omit those which are not metallic (e.g., Sc_2CCl_2 [24]), or have been synthesized without reports for superconducting behavior so far (e.g., Ti_2CCl_2 or Zr_2CCl_2 [27]). The remaining compounds Zr_2NCl_2 , Sc_2NCl_2 and Zr_2NS_2 are thus selected for this study, where we look for enhanced T_c values in these functionalized compounds in contrast to their bare forms. For completeness, we remark that we have also attempted to compute Sc_2NS_2 which however resulted in unstable structure with imaginary phonon frequencies and hence is not included in this paper. In addition, several levels of tensile strain are also applied on Zr_2NCl_2 and Zr_2NS_2 to demonstrate the possibility of strain-induced T_c enhancement.

Computationally, density functional theory (DFT) and density functional perturbation theory (DFPT) are often utilized for searching new superconductor candidates. Combined with the McMillan formula [11], a phenomenological expression for the transition temperature T_c is given by:

$$T_c = \frac{\omega_{\text{ln}}}{1.2} \exp \left[\frac{-1.04(1 + \lambda)}{\lambda - \mu^*(1 + 0.62\lambda)} \right] \quad (1)$$

where the electron-phonon coupling constant λ and the averaged phonon frequency ω_{ln} are obtainable from standard DFPT routine. The effect of screened Coulomb pseudopotential is parametrized by μ^* , whose value is usually specified around 0.1 – 0.15 [28, 29]. However, the need for such empirical choice limits the predictive power of the McMillan formula. Moreover, the superconducting gap profile is inaccessible by this approach. Although it is possible to solve for the gap with the Migdal-Eliashberg (ME) formalism [30, 31], this method still requires the user to empirically specify the μ^* value in practice. Hence, we turn to the density functional theory for superconductors (SCDFT) [32–36] as it solves the gap equation for T_c without the need for empirical parameters. This SCDFT trait thus differentiates our work from other studies derived from the McMillan and Migdal-Eliashberg approaches.

This paper follows a similar strategy to preceding works [9, 10, 26] in exploring possible superconductivity in functionalized MXenes. Section II outlines the computational methods. Section III computes the configuration in Figure 1 for T_c of the target compounds. The T_c trend is compared against electron-phonon coupling constant λ , electron density of states at Fermi level $N(E_F)$ (states/eV), and averaged Coulomb interaction μ_C to look for correlations. As with previous works [3, 9, 10, 26], we shall find that λ best correlates with T_c . The changes upon functionalization or applied strain are analyzed from the modified electronic bandstructure and phonon dispersion. The effects of ferromagnetic spin-fluctuations (SF) are also briefly discussed. Section IV concludes the paper.

II. COMPUTATIONAL METHODS

Normal-state DFT and DFPT calculations are carried out with QUANTUM ESPRESSO code [37–39]. Exchange–correlation effects are treated with the generalized gradient approximation (GGA) using the Perdew – Burke – Ernzerhof (PBE) functional [40]. A vacuum of at least 15 Å is included in the unit cell. We use ultra-soft pseudopotentials from PSLibrary [41]. The structure relaxation is performed with energy and force convergence thresholds of 10^{-6} and 10^{-5} in Ry atomic units, under 0.003675 Ry Gaussian smearing. The energy cutoff for wave function and charge density are 80 Ry and 640 Ry, respectively. SCDFT calculation is carried out with the SUPERCONDUCTING-TOOLKIT code [34]. For this procedure, the self-consistent charge density calculation uses the optimized tetrahedron method [42]. Spin-orbit interaction (SOI) effects in MXenes are expected to be minor for Zr_2N and Sc_2N -based compounds and thus are omitted here [3]. In this approach, the T_c is obtained by solving the SCDFT gap equation,

$$\Delta_{n\mathbf{k}} = -\frac{1}{2} \sum_{n'\mathbf{k}'} \frac{K_{n\mathbf{k}n'\mathbf{k}'}(\xi_{n\mathbf{k}}, \xi_{n'\mathbf{k}'})}{1 + Z_{n\mathbf{k}}(\xi_{n\mathbf{k}})} \times \frac{\Delta_{n'\mathbf{k}'}}{\sqrt{\xi_{n'\mathbf{k}'}^2 + \Delta_{n'\mathbf{k}'}^2}} \tanh \left(\frac{\sqrt{\xi_{n'\mathbf{k}'}^2 + \Delta_{n'\mathbf{k}'}^2}}{2T} \right) \quad (2)$$

where $\xi_{n\mathbf{k}}$ is the Kohn-Sham eigenvalue measured from the Fermi level E_F at the band index n and wavenumber \mathbf{k} . T_c is the temperature where the superconducting gap $\Delta_{n\mathbf{k}}$ vanishes at all n and \mathbf{k} . $K_{n\mathbf{k}n'\mathbf{k}'}$ is an integration kernel made of interaction terms, for instance:

$$K_{n\mathbf{k}n'\mathbf{k}'} = K_{n\mathbf{k}n'\mathbf{k}'}^{\text{ep}} + K_{n\mathbf{k}n'\mathbf{k}'}^{\text{ee}} \quad (3)$$

consists of the electron-phonon $K_{n\mathbf{k}n'\mathbf{k}'}^{\text{ep}}$ and the (screened) electron-electron interaction $K_{n\mathbf{k}n'\mathbf{k}'}^{\text{ee}}$ terms. Similarly, $Z_{n\mathbf{k}}$ is a renormalization factor that arises from such interactions. Approximations to $K_{n\mathbf{k}n'\mathbf{k}'}$ and $Z_{n\mathbf{k}}$ have been derived over the years [32–35, 43]. We use the electron-phonon kernels of Ref. [35] and the screened electron-electron interaction kernel based on random phase approximation (RPA) from Ref. [34]. Following Ref. [34], at least 20 empty bands are included in the screened Coulomb interaction calculation procedure.

TABLE I. The \mathbf{k} - and \mathbf{q} -point grids for SCDFT procedure.

Calculation steps	\mathbf{k} - and \mathbf{q} -point grids
self-consistent charge density	\mathbf{k} : medium grid
phonons (DFPT)	\mathbf{k} : medium; \mathbf{q} : coarse
electron-phonon coupling	\mathbf{k} : coarse; \mathbf{q} : coarse
Energy dispersion (one-shot)	\mathbf{k} : fine grid
Kohn-Sham orbitals (one-shot)	twin \mathbf{k} -point grids
screened Coulomb interaction	\mathbf{q} : coarse grid
SCDFT gap equation	\mathbf{k} : coarse grid

The information about the \mathbf{k} - and \mathbf{q} -point grids for each SCDFT procedure step [34] is summarized in Table

I. For Nb_2C systems, Sc_2NCl_2 and Zr_2NCl_2 , $8 \times 8 \times 1$, $16 \times 16 \times 1$, and $32 \times 32 \times 1$ are used as the coarse, medium, and fine grid densities. 128 \mathbf{k} -points are used for the twin grids. For Zr_2N and Zr_2NS_2 , the coarse, medium, and fine grid densities are increased to $10 \times 10 \times 1$, $20 \times 20 \times 1$, and $40 \times 40 \times 1$ with twin grids of 200 \mathbf{k} -points to improve convergence. We generally follow the study of elemental superconductors [34], in which a satisfactory convergence of the results was demonstrated with similar parameters.

III. RESULTS AND DISCUSSIONS

A. T_c of Nb_2C , Nb_2CCl_2 , and Nb_2CS_2

First, we briefly check our approach against experiment [4] and calculations based on McMillan formula [3, 9, 10] for Nb_2C , Nb_2CCl_2 , and Nb_2CS_2 in Table II.

TABLE II. The superconducting transition temperature T_c (K) of Nb_2C , Nb_2CCl_2 and Nb_2CS_2 .

T_c (K)	Experiment [4]	DFT-McMillan [3, 9, 10]	SCDFT (this work)
Nb_2C	less than 2 K	less than 1 K	less than 2 K
Nb_2CCl_2	6.0	9.6	8.2
Nb_2CS_2	6.4	10.7	8.4

Our T_c values are comparable to experiment [4] and DFT-McMillan results [3, 9, 10]. The relative T_c trend, i.e., $T_c(\text{Nb}_2\text{C}) < T_c(\text{Nb}_2\text{CCl}_2) \lesssim T_c(\text{Nb}_2\text{CS}_2)$ is also captured. This supports the conjectured phonon-mediated mechanism in these materials [3, 6, 9, 10, 26]. Having confirmed the applicability of SCDFT for functionalized Nb_2C , we use it next for exploring Zr_2N and Sc_2N -based materials.

B. Functionalized Sc_2N and Zr_2N compounds

1. Overview

The computed values for T_c , λ , $N(E_F)$, and μ_C for the MXenes studied in this paper are provided in Table III.

TABLE III. The superconducting transition temperature T_c (K), electron-phonon coupling constant λ , electron density of states at Fermi level $N(E_F)$ (state/eV), and averaged Coulomb interaction μ_C for functionalized MXene compounds studied in this paper.

Compounds	T_c	λ	$N(E_F)$	μ_C
Sc_2NCl_2	1.79	0.31	1.44	0.27
Zr_2NCl_2	2.16	0.33	1.18	0.20
Zr_2NS_2	9.48	0.60	1.25	0.19

Note that μ_C is a different quantity to the empirical parameter μ^* . They can be expressed as,

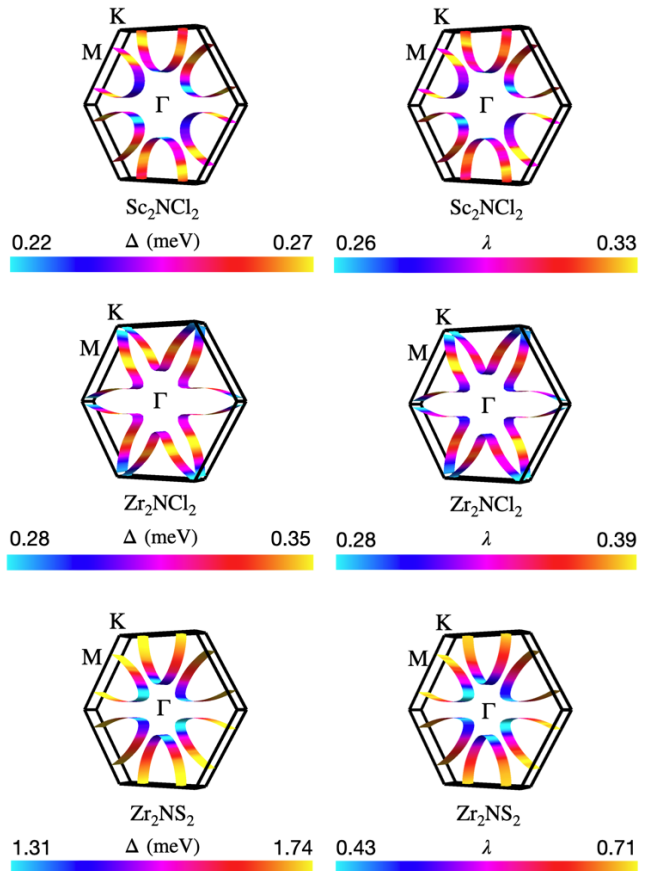


FIG. 2. The electron-phonon coupling λ and superconducting gap Δ profiles at the Fermi surface across the Brillouin zone for Sc_2NCl_2 , Zr_2NCl_2 , and Zr_2NS_2 at 1 K.

$$\mu_C = N(E_F) \langle K_{nkn'k'}^{ee} \rangle \quad (4)$$

$$\mu^* = \frac{\mu_C}{1 + \mu_C \ln \frac{E_c}{\omega_c}} \quad (5)$$

where $\langle \rangle$ indicates a Fermi surface average, E_c and ω_c are electronic and phononic cutoff energies whose values may be arbitrarily specified [44, 45]. This ambiguity makes it less meaningful to compare μ^* values computed in this way against the customary values of 0.1 - 0.15 in the McMillan formalism [36, 45]. Instead, comparing the values of μ_C is preferred [45]. We find our μ_C values to be comparable to those of elemental superconductors [34]. The T_c values trend better with λ than $N(E_F)$. This agrees with the cases for Nb_2C [9, 10] and for superconducting bare MXenes [3]. We also note that T_c does not trend with lattice parameters (see Table S1 of Supplemental Material for crystal structure data [46]).

The profiles for λ and SCDFT gap Δ at the Fermi surface across the Brillouin zone are shown in Figure 2. One commonality is observed: Δ has larger values in areas where high λ values can be found, and vice versa.

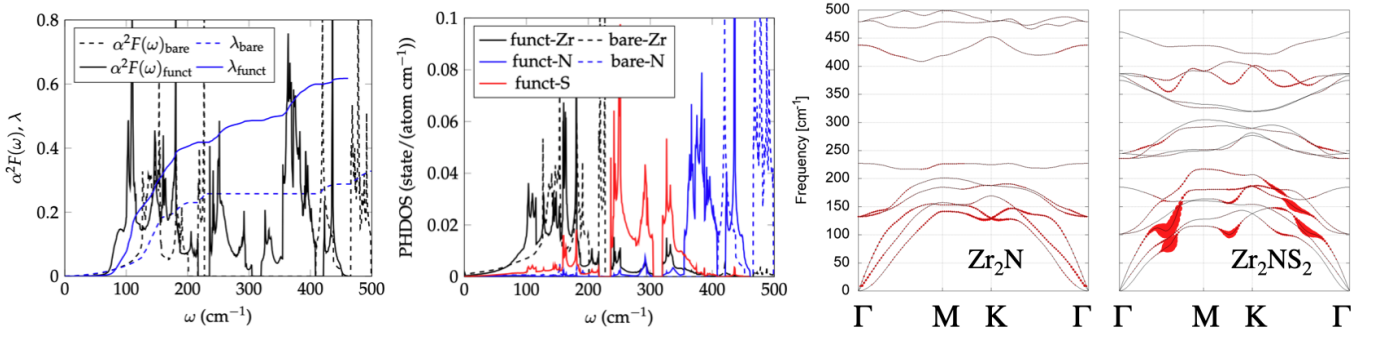


FIG. 3. **Left:** Eliashberg spectral function $\alpha^2 F(\omega)$, electron-phonon coupling λ , and partial phonon density of states (PHDOS) for the bare (dashed lines) and S-functionalized Zr_2N MXenes (solid lines). **Right:** Comparison of the phonon bandstructures (solid black lines). The red-colored circles are scaled equally for both compounds to their phonon-dependent electron-phonon coupling constants $\lambda_{\mathbf{q}\nu}$ across the Brillouin zone.

We also plot Δ as a function of temperature T in Figure S1 of Supplemental Material [46]. The compounds seem to follow similar gradually decreasing curves apart from the size of the gap.

2. Understanding λ enhancement in functionalized Zr_2N

We compare Zr_2N and Zr_2NS_2 systems to illustrate the effects of functionalization in improving λ . Let us first consider the following expression for λ [26, 37, 38]:

$$\lambda = 2 \int \frac{\alpha^2 F(\omega)}{\omega} d\omega \quad (6)$$

and the isotropic Eliashberg spectral function,

$$\alpha^2 F(\omega) = \frac{1}{N(E_F)} \sum_{\nu, \mathbf{k}, \mathbf{q}} |g_{\mathbf{k}, \mathbf{k}+\mathbf{q}}^\nu|^2 \delta(\omega - \omega_{\mathbf{q}}^\nu) \delta(\varepsilon_{\mathbf{k}}) \delta(\varepsilon_{\mathbf{k}+\mathbf{q}}) \quad (7)$$

with the electron-phonon matrix elements ($g_{\mathbf{k}, \mathbf{k}+\mathbf{q}}^\nu$), phonon ($\omega_{\mathbf{q}}^\nu$, mode index ν) and electron ($\varepsilon_{\mathbf{k}}$, measured from Fermi level) bandstructures obtained from standard DFT+DFPT routines. Based on Eqs. (6)-(7), we focus on low-frequency phonons to analyze the changes in λ .

The isotropic Eliashberg spectral function and its corresponding λ for Zr_2N and Zr_2NS_2 are compared in Figure 3. Before proceeding further, we remark here that these plots are computed separately from the SCDFPT calculations in Table III. In particular, the interpolation method [37, 38, 47] which enables efficient electron-phonon calculations using unshifted \mathbf{q} -point grids is used instead of the tetrahedron method at the DFPT step. A slight difference may hence exist in the λ values relative to Table III, but the physical insights we draw from these results should remain unaffected. We use a broadening parameter of 0.033 Ry, similar to Ref. [47]. We find this choice yields λ value for Zr_2NS_2 of approximately 0.62, which are quite close to the SCDFPT-obtained value of 0.6 in Table III. Most of the λ values are accumulated at low frequencies, with λ of Zr_2NS_2 having reached 0.4

(2/3 of the total λ) under the frequencies of 200 cm^{-1} , confirming the importance of low-frequency phonons. In this regime, $\alpha^2 F(\omega)$ has more spectral weight for Zr_2NS_2 than the bare compound. The λ further increases to approximately 0.6 as the frequency reaches $\omega = 400 \text{ cm}^{-1}$, in which a significant amount $\alpha^2 F(\omega)$ spectral weight is present for the functionalized compound.

The aforementioned changes can be explained by comparing the partial phonon density of states (PHDOS) and the phonon dispersion shown in Figure 3. First, the S-contributed phonon states can be identified around $\omega \approx 250 - 350 \text{ cm}^{-1}$. We note the Zr- and N-dominant phonon states for $\omega < 200 \text{ cm}^{-1}$ and $\omega \approx 350 - 400 \text{ cm}^{-1}$ having shifted from higher frequencies compared to the bare compound. These phonon softening can also be observed from the phonon dispersion plots. The PHDOS peaks may be explained by additional flat band sections and optimum points in the phonon dispersion, such as the one located just above $\omega \approx 100 \text{ cm}^{-1}$ between M and K point. We also visualize the estimated phonon-dependent electron-phonon coupling constant $\lambda_{\mathbf{q}\nu} = \frac{1}{\pi N(E_F)} \frac{\gamma_{\mathbf{q}\nu}}{\omega_{\mathbf{q}}^2}$ by scaling them to the red-colored marker size drawn on the dispersion lines. Unlike in the bare compound, the value of $\lambda_{\mathbf{q}\nu}$ is larger at parts of the dispersion with local minima at low frequencies. This finding is understandable considering the shape of the electronic Fermi surface of Zr_2NS_2 and also that local minimas in the phonon dispersion often translate to large phonon density of states.

Next, the projected electronic bandstructures of Zr_2N and Zr_2NS_2 are shown in Figure 4. The Fermi level shifts to a lower energy, which suggests hole doping upon functionalization. The flat sections at Γ and near K point in the bare compound are pushed above E_F in Zr_2NS_2 , which can explain its reduced $N(E_F)$ value from 3.7 state/eV to 1.25 state/eV. There are significant contributions of S atoms at the Fermi surface between M and K points. As we do find between these points also a modified phonon dispersion (c.f., Figure 3) with high λ and Δ values (c.f., Figure 2), hybridization between Zr and S bands might be a factor that contributes to such effects.

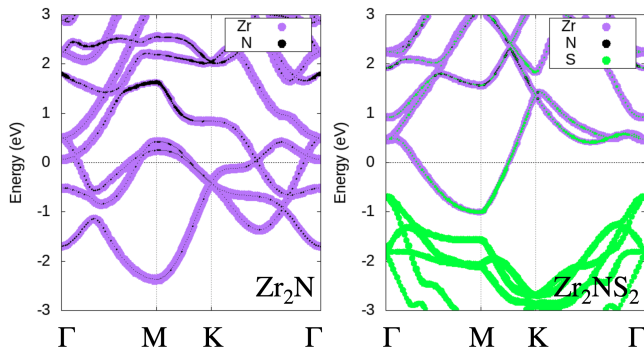


FIG. 4. Projected electronic bandstructure of Zr_2N and Zr_2NS_2 . Purple, black, and green circles denote Zr, N, and S contributions, respectively.

3. Analyzing the T_c difference between Sc_2NCl_2 and Zr_2NS_2

From Table III, we note that there is a significant difference between the T_c values of Sc_2NCl_2 (1.79 K) and Zr_2NS_2 (9.48 K). This finding is interesting as their general shape of the Fermi surface is quite similar (see Figure 2). Furthermore, Sc_2NCl_2 has higher density of states at Fermi level as well as a smaller atomic mass than Zr_2NS_2 . These traits may suggest that Sc_2NCl_2 should be having higher T_c values than Zr_2NS_2 instead. Hence, we believe it is worthwhile to discuss more about the low T_c of Sc_2NCl_2 predicted by our calculations here.

In Figure 2, we can read the superconducting gap and the electron-phonon coupling profile across the Fermi surface. Although there is a similarity in the Fermi surface shape, the superconducting gap size and its anisotropy are larger for Zr_2NS_2 relative to Sc_2NCl_2 . These properties correlate with the electron-phonon coupling profile and are likely due to the interactions between the transition metal and functional group atoms near the Fermi level. As discussed in the previous subsection, the S-phonon states seem to shift the Zr and N phonon states in Zr_2NS_2 quite significantly toward lower frequencies. This was not quite the case for Sc_2NCl_2 , where only a small fraction of the phonon states is found below $\omega = 150 \text{ cm}^{-1}$ (see Figure S2 of Supplemental Material [46]).

The projected electronic band structure for Sc_2NCl_2 is shown in Figure 5. We compare the band structure contributions from functional group atoms at the Fermi level between Sc_2NCl_2 and Zr_2NS_2 . While S has a significant presence in the valence band of Zr_2NS_2 (see Figure 4), the presence of Cl in the valence band of Sc_2NCl_2 is more subtle. As suggested in the previous section, we believe this difference may be responsible for the distinct electron-phonon coupling strength between the two compounds which ultimately affects the superconducting gap anisotropy as well as the T_c value.

On the other hand, we may also compare the Cl-functionalized compounds in which their Cl presence at the valence band is subtle: Sc_2NCl_2 and Zr_2NCl_2 (see Figure 5). From Table III, the T_c and λ values are

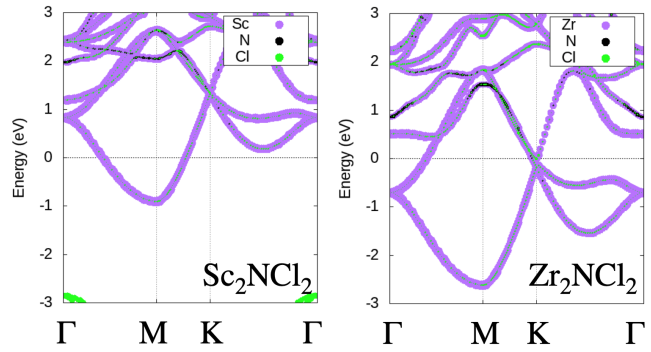


FIG. 5. Projected electronic bandstructure of Sc_2NCl_2 and Zr_2NCl_2 . Purple, black, and green circles denote Sc/Zr, N, and Cl contributions, respectively.

quite comparable to each other. The profiles in Figure 2 are also similar in both magnitude and anisotropy. The slightly lower T_c for Sc_2NCl_2 may be explained by the stronger electron-electron interaction parametrized by μ_C . Together with the previous comparison to Zr_2NS_2 , this observation suggests that the T_c difference between these compounds might be indicated by the extent of each functional group's presence at the Fermi level.

Usually, the T_c value may be increased by improving the electronic density of states $N(E_F)$ or the electron-phonon coupling. Because the bandstructure of bare MXenes may consist of several flat sections (see Figure 4), they can have higher value of $N(E_F)$ than their functionalized counterparts. However, many bare MXenes are not expected to superconduct due to their small λ values despite having large density of states [3]. Hence, we believe λ has a bigger role than $N(E_F)$ in determining T_c for these materials. The lower T_c value of Sc_2NCl_2 despite its higher $N(E_F)$ relative to Zr_2NS_2 can therefore be explained in this framework.

4. Strain-induced T_c enhancement

We move to discuss the effects of applied tensile strain. As we could not afford a comprehensive strain optimization exercise for these materials due limited computational resources, we shall aim to demonstrate the possibility of strain-induced T_c enhancement in a simple exercise for functionalized Zr_2N MXenes as follows.

We begin by computing a selected compound (e.g. Zr_2NS_2) with an arbitrary strain value (e.g. 6%) and compare its $N(E_F)$ value against the unstrained system. We then proceed to calculate its phonon dispersion if there is an increase in $N(E_F)$ value. The remaining SCDFC calculations are carried out only if no imaginary phonon frequencies are found. Otherwise, we reduce the strain level and repeat this cycle until these conditions are satisfied. For Zr_2NS_2 and Zr_2NCl_2 , we arrive at the suitable strain level of 2% and 6% respectively.

We list the T_c , λ , $N(E_F)$, and μ_C values on the selected

TABLE IV. The superconducting transition temperature T_c (K), electron-phonon coupling constant λ , electron density of states at Fermi level $N(E_F)$ (state/eV), and averaged Coulomb interaction μ_C for strained Zr_2NCl_2 and Zr_2NS_2 .

Compounds	T_c	λ	$N(E_F)$	μ_C
Zr_2NCl_2 (6% strain)	4.22	0.46	1.45	0.23
Zr_2NS_2 (2% strain)	11.58	0.76	1.37	0.20

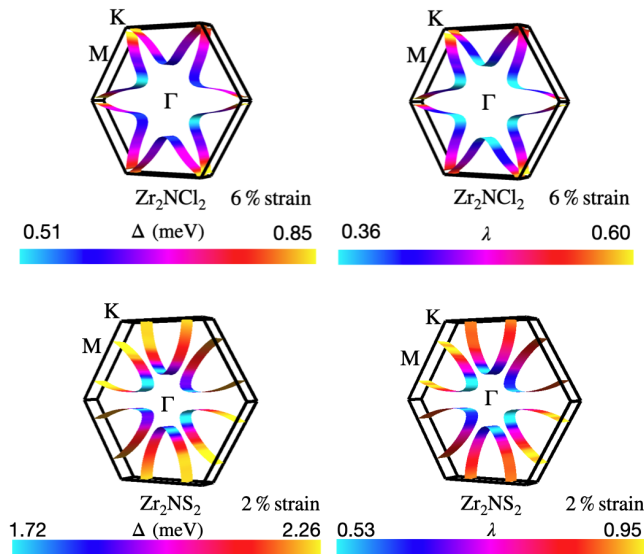


FIG. 6. The superconducting gap Δ and the electron-phonon coupling λ profiles at the Fermi surface across the Brillouin zone for Zr_2NCl_2 with 6% strain, and Zr_2NS_2 with 2% strain at 1 K.

strained compounds in Table IV, which are higher compared to their unstrained counterparts. The anisotropy in Δ and λ are also enhanced, in particular for Zr_2NCl_2 with high values near the K point (Figure 6).

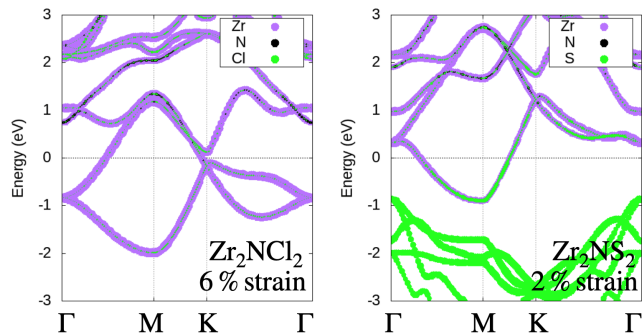


FIG. 7. Projected electronic bandstructures for Zr_2NCl_2 (6% strain) and Zr_2NS_2 (2% strain). Purple, black, and green circles denote Zr, N, and Cl/S contributions, respectively.

We plot the projected electronic bandstructure in Figure 7. The Zr_2NS_2 bandstructure does not show major changes for the valence band profile, which is not sur-

prising as the applied strain is small. However, the bandstructure profile changes for Zr_2NCl_2 near E_F around the K point, as it shows a flatter profile consistent with its increased $N(E_F)$. The functional group atoms still contribute to the valence band, with the contributions from S being larger than Cl for their respective compounds. Similar to our previous analysis, we note a shift of Zr phonon dispersion toward lower frequencies for both compounds. (Figures S3 and S4 of Supplemental Material [46]). The enhanced λ values may thus be considered as a result from these changes in electronic and phononic bandstructure.

C. Spin-fluctuation effects

We briefly discuss the effects of including ferromagnetic spin fluctuations (SF) [48, 49] as additional terms in the SCDFT exchange-correlation kernels, $K_{nk'n'\mathbf{k}'}^{SF}$ and Z_{nk}^{SF} as implemented in the SUPERCONDUCTING-TOOLKIT code [34]. Following Refs. [49, 50], SF may hinder the phonon-mediated pairing of electrons with opposite spins and effectively reduce T_c . Using the same computational parameters as the non-SF case, we show in Table V the SF-corrected superconducting transition temperature T_c^{SF} (K) and the Fermi surface average of SF kernel μ_S (c.f., Eq. (4)) [34] as well as the effective electron-electron interaction $\mu_C + \mu_S$ for our compounds.

TABLE V. The computed SF-corrected superconducting transition temperature T_c^{SF} (K), averaged SF kernel μ_S and effective electron-electron interaction $\mu_C + \mu_S$.

Compounds	T_c^{SF}	μ_S	$\mu_C + \mu_S$
Sc_2NCl_2	0.89	0.06	0.33
Zr_2NCl_2	1.37	0.04	0.24
Zr_2NS_2	8.14	0.03	0.22

The SF inclusion does not affect the calculation of λ or $N(E_F)$. However, SF leads to reduced T_c^{SF} values for all compounds. This reduction is likely due to the increased effective electron-electron interaction $\mu_C + \mu_S$. Although the T_c^{SF} values of Zr_2NCl_2 and Sc_2NCl_2 are reduced below 2 K, the T_c^{SF} for Zr_2NS_2 remains above 8 K. Hence, this result adds confidence in Zr_2NS_2 as a potential superconducting candidate.

In the prior SCDFT study for elemental superconductors, superconductivity for elemental Sc is completely suppressed ($T_c : 2.7 \rightarrow 0$ K) by including SF effects [34]. This suppression is likely due to Sc's high μ_S value (0.97), which in turn may be caused by the localized 3d orbital and its high density of states (2.01 states/eV) [34]. On the other hand, our compounds in Table V have smaller μ_S values which cause their superconductivity not to be fully suppressed. This difference in μ_S values may be due to several interrelated factors as follows.

First, our MXene compounds have smaller density of states at the Fermi level [$N(E_F) < 1.5$ state/eV, see

Table III]. Next, the electron configuration of Zr has valence electrons in the $4d$ orbital. The delocalization of electronic orbitals increases with the principal quantum number $3d \rightarrow 4d$, and SF effects should be weaker in less localized orbitals [34, 49]. Furthermore, the MXene valence band is also contributed by N, Cl, and S atoms. The valence configurations of these atoms are made of s and p orbitals, which are less localized than the $3d$ orbital of elemental Sc. We also observe that these compounds do not have many flat sections in their electronic bandstructure at the Fermi level. Since flat band sections indicate strong localization with typically high $N(E_F)$, their absence is in agreement for a more delocalized picture that leads to a small SF parameter μ_S .

Nevertheless, we remark that SF calculations are more sensitive to computational parameters and thus often requires higher cutoff energies to be precisely computed than non-SF calculations. Unfortunately, this complexity may cause the computational costs to become prohibitive, even for simple elemental superconductors. More resources are required for 2D compounds as vacuum must be included in the computational cell. As such, our SF study should be regarded only as a qualitative exercise. In the case of elemental Scandium, its T_c is completely suppressed with SF effects. Thus, SF can qualitatively change the predicted property for a material from superconducting to non-superconducting. By performing our simple SF calculations, we simply wish to verify whether our compounds, especially Zr_2NS_2 , remain good superconductor candidates even when SF effects are included. As reflected in Table V, this seems to be the case as Zr_2NS_2 remains with a sufficiently high T_c^{SF} which can be reasonably measured in experiments.

D. Possible extensions

The examples presented in this brief study are not intended to be exhaustive. Wider choices of functional groups or MXene compounds may be explored with the help of structure prediction algorithms (e.g., Ref. [51]), and further refinements to the SCDFT calculations may be opted with added complexities. Inclusion of van der Waals corrections may also be pursued if a suitable exchange-correlation functional can be identified. MXene layers are reported to be only weakly coupled in prior studies [9, 10]. For Nb_2C systems, attempts [9, 10] to include van der Waals corrections based on Grimme's DFT-D2 [52], DFT-D3 [53], and Becke-Johnson method [54] were not successful. Careful treatment of van der Waals effects is a desirable extension in future studies.

IV. CONCLUSIONS

In this paper, we explore several new superconductor candidates in functionalized MXenes beyond the Nb_2C system. Functionalized Zr_2N and Sc_2N with Cl and S surface terminations are studied with *ab initio* calculations based on density functional theory for superconductors (SCDFT). This method allows T_c to be computed without empirical parameters, hence differentiating this study from prior works [3, 9, 10, 26]. The T_c is predicted to reach as high as 9.48 K for Zr_2NS_2 , while further T_c improvements may be achieved with applied strain. The T_c trends with λ , whose profile across the Fermi surface resembles that of Δ . The λ enhancement is suggested to come from modified phonon dispersion and electronic bandstructure. Hybridization between the transition metal and functional group atoms may induce such modifications, as reflected from their mixed contributions in the electronic bandstructure at the Fermi level. We encourage further research to explore more functionalized MXene compounds as superconductor candidates.

AUTHOR CONTRIBUTIONS

Alpin N. Tatan: Conceptualization, Methodology, Formal analysis, Investigation, Writing - original draft, Writing - review and editing. **Osamu Sugino:** Funding acquisition, Supervision, Writing - review and editing.

CONFLICTS OF INTEREST

There are no conflicts to declare.

DATA AVAILABILITY

The data supporting this article have been included as part of the Supplemental Material [46].

ACKNOWLEDGMENTS

The calculations were performed with the facilities of the Supercomputer Center, the Institute for Solid State Physics, the University of Tokyo.

[1] A. VahidMohammadi, J. Rosen, and Y. Gogotsi, The world of two-dimensional carbides and nitrides (MXenes), *Science* **372**, eabf1581 (2021).

[2] M. Khazaei, A. Ranjbar, M. Arai, T. Sasaki, and S. Yunoki, Electronic properties and applications of MXenes: a theoretical review, *J. Mater. Chem. C* **5**, 2488 (2017).

- [3] J. Bekaert, C. Sevik, and M. V. Milošević, First-principles exploration of superconductivity in MXenes, *Nanoscale* **12**, 17354 (2020).
- [4] V. Kamysbayev, A. S. Filatov, H. Hu, X. Rui, F. Lagunas, D. Wang, R. F. Klie, and D. V. Talapin, Covalent surface modifications and superconductivity of two-dimensional metal carbide MXenes, *Science* **369**, 979 (2020).
- [5] K. Wang, H. Jin, H. Li, Z. Mao, L. Tang, D. Huang, J.-H. Liao, and J. Zhang, Role of surface functional groups to superconductivity in Nb₂C-MXene: Experiments and density functional theory calculations, *Surfaces and Interfaces* **29**, 101711 (2022).
- [6] H. Pazniak, T. Ouisse, U. Wiedwald, J. Gonzalez-Julian, T. Ito, F. Wilhelm, A. Rogalev, and S. Quessada, Electronic and thermal properties of Nb₂CCl₂ MXenes, *Open Ceramics* **18**, 100579 (2024).
- [7] X. Xu, C. Zhang, J. Yin, J. Smajic, M. Bahabri, Y. Lei, M. N. Hedhili, M. K. Hota, L. Shi, T. Guo, *et al.*, Anisotropic superconducting Nb₂CT_x MXene processed by atomic exchange at the wafer scale, *Adv. Mater.* **36**, 2305326 (2024).
- [8] M. Jiang, D. Wang, Y.-H. Kim, C. Duan, D. Talapin, and C. Zhou, Evolution of surface chemistry in two-dimensional MXenes: from mixed to tunable uniform terminations, *Angew. Chem. Int. Ed.*, e202409480 (2024).
- [9] C. Sevik, J. Bekaert, and M. V. Milošević, Superconductivity in functionalized niobium-carbide mxenes, *Nanoscale* **15**, 8792 (2023).
- [10] C. Sevik, J. Bekaert, and M. V. Milošević, Correction: Superconductivity in functionalized niobium-carbide mxenes, *Nanoscale* **15**, 11727 (2023).
- [11] W. L. McMillan, Transition temperature of strong-coupled superconductors, *Phys. Rev.* **167**, 331 (1968).
- [12] E. Dagotto, J. Burgy, and A. Moreo, Nanoscale phase separation in colossal magnetoresistance materials: lessons for the cuprates?, *Solid State Commun.* **126**, 9 (2003).
- [13] R. Zhang, C. Lane, B. Singh, J. Nokelainen, B. Barbiellini, R. S. Markiewicz, A. Bansil, and J. Sun, Magnetic and f-electron effects in LaNiO₂ and NdNiO₂ nickelates with cuprate-like $3d_{x^2-y^2}$ band, *Commun. Phys.* **4**, 118 (2021).
- [14] Y. Ji, J. Liu, L. Li, and Z. Liao, Superconductivity in infinite layer nickelates, *J. Appl. Phys.* **130**, 060901 (2021).
- [15] W. E. Pickett, Electronic structure of the high-temperature oxide superconductors, *Rev. Mod. Phys.* **61**, 433 (1989).
- [16] J. Nokelainen, C. Lane, R. S. Markiewicz, B. Barbiellini, A. Pulkkinen, B. Singh, J. Sun, K. Pussi, and A. Bansil, *Ab initio* description of the Bi₂Sr₂CaCu₂O_{8+δ} electronic structure, *Phys. Rev. B* **101**, 214523 (2020).
- [17] J. W. Furness, Y. Zhang, C. Lane, I. G. Buda, B. Barbiellini, R. S. Markiewicz, A. Bansil, and J. Sun, An accurate first-principles treatment of doping-dependent electronic structure of high-temperature cuprate superconductors, *Commun. Phys.* **1**, 1 (2018).
- [18] A. N. Tatan, J. Haruyama, and O. Sugino, First-principles electronic structure investigation of HgBa₂Ca_{n-1}Cu_nO_{2n+2+x} with the SCAN density functional, *AIP Advances* **12**, 105308 (2022).
- [19] Y. Zhang, C. Lane, J. W. Furness, B. Barbiellini, J. P. Perdew, R. S. Markiewicz, A. Bansil, and J. Sun, Competing stripe and magnetic phases in the cuprates from first principles, *Proc. of the Nat'l Acad. of Sci.* **117**, 68 (2020).
- [20] N. P. Armitage, P. Fournier, and R. L. Greene, Progress and perspectives on electron-doped cuprates, *Rev. Mod. Phys.* **82**, 2421 (2010).
- [21] P. Fournier, T' and infinite-layer electron-doped cuprates, *Physica C* **514**, 314 (2015).
- [22] A. N. Tatan, J. Haruyama, and O. Sugino, Magnetic phases of electron-doped infinite-layer Sr_{1-x}La_xCuO₂ from first-principles density functional calculations, *Phys. Rev. B* **109**, 165134 (2024).
- [23] Y. Nomura and R. Arita, Superconductivity in infinite-layer nickelates, *Rep. Prog. Phys.* **85**, 052501 (2022).
- [24] Y. Qin, X.-H. Zha, X. Bai, K. Luo, Q. Huang, Y. Wang, and S. Du, Structural, mechanical and electronic properties of two-dimensional chlorine-terminated transition metal carbides and nitrides, *J. Phys.: Condens. Matter* **32**, 135302 (2020).
- [25] X. Lu, J. Qi, J. Ren, J. Li, H. Xue, F. Tang, and X. Guo, First-principles study of the effect of O and S functional groups on the lithium storage properties of Zr₂N materials, *J. Mater. Chem. C* **12**, 2227 (2024).
- [26] J. Bekaert, C. Sevik, and M. V. Milošević, Enhancing superconductivity in MXenes through hydrogenation, *Nanoscale* **14**, 9918 (2022).
- [27] Di Wang and Chenkun Zhou and Alexander S. Filatov and Wooje Cho and Francisco Lagunas and Mingzhan Wang and Suriyanarayanan Vaikuntanathan and Chong Liu and Robert F. Klie and Dmitri V. Talapin, Direct synthesis and chemical vapor deposition of 2D carbide and nitride MXenes, *Science* **379**, 1242 (2023).
- [28] P. Morel and P. W. Anderson, Calculation of the superconducting state parameters with retarded electron-phonon interaction, *Phys. Rev.* **125**, 1263 (1962).
- [29] K. Sano, M. Seo, and K. Nakamura, Plasmon Effect on the Coulomb pseudopotential μ^* in the McMillan equation, *J. Phys. Soc. Jpn.* **88**, 093703 (2019).
- [30] H. Lee, S. Poncé, K. Bushick, S. Hajinazar, J. Lafuente-Bartolome, J. Leveillee, C. Lian, J.-M. Lihm, F. Macheda, H. Mori, *et al.*, Electron-phonon physics from first principles using the EPW code, *npj Comput. Math.* **9**, 156 (2023).
- [31] E. R. Margine and F. Giustino, Anisotropic Migdal-Eliashberg theory using Wannier functions, *Phys. Rev. B* **87**, 024505 (2013).
- [32] M. Lüders, M. A. L. Marques, N. N. Lathiotakis, A. Floris, G. Profeta, L. Fast, A. Continenza, S. Massidda, and E. K. U. Gross, *Ab initio* theory of superconductivity. I. Density functional formalism and approximate functionals, *Phys. Rev. B* **72**, 024545 (2005).
- [33] M. A. L. Marques, M. Lüders, N. N. Lathiotakis, G. Profeta, A. Floris, L. Fast, A. Continenza, E. K. U. Gross, and S. Massidda, *Ab initio* theory of superconductivity. II. Application to elemental metals, *Phys. Rev. B* **72**, 024546 (2005).
- [34] M. Kawamura, Y. Hizume, and T. Ozaki, Benchmark of density functional theory for superconductors in elemental materials, *Phys. Rev. B* **101**, 134511 (2020).
- [35] A. Sanna, C. Pellegrini, and E. K. U. Gross, Combining Eliashberg theory with density functional theory for the accurate prediction of superconducting transition temperatures and gap functions, *Phys. Rev. Lett.* **125**, 057001 (2020).

- [36] M. Kawamura, R. Akashi, and S. Tsuneyuki, Anisotropic superconducting gaps in $\text{YNi}_2\text{B}_2\text{C}$: A first-principles investigation, *Phys. Rev. B* **95**, 054506 (2017).
- [37] P. Giannozzi, S. Baroni, N. Bonini, M. Calandra, R. Car, C. Cavazzoni, D. Ceresoli, G. L. Chiarotti, M. Cococcioni, I. Dabo, *et al.*, QUANTUM ESPRESSO: a modular and open-source software project for quantum simulations of materials, *J. Phys.: Condens. Matter* **21**, 395502 (2009).
- [38] P. Giannozzi, O. Andreussi, T. Brumme, O. Bunau, M. Buongiorno Nardelli, M. Calandra, R. Car, C. Cavazzoni, D. Ceresoli, M. Cococcioni, *et al.*, Advanced capabilities for materials modelling with Quantum ESPRESSO, *J. Phys.: Condens. Matter* **29**, 465901 (2017).
- [39] T. Sohler, M. Calandra, and F. Mauri, Density functional perturbation theory for gated two-dimensional heterostructures: Theoretical developments and application to flexural phonons in graphene, *Phys. Rev. B* **96**, 075448 (2017).
- [40] J. P. Perdew, K. Burke, and M. Ernzerhof, Generalized gradient approximation made simple, *Phys. Rev. Lett.* **77**, 3865 (1996).
- [41] A. Dal Corso, Pseudopotentials periodic table: From H to Pu, *Comput. Mater. Sci.* **95**, 337 (2014).
- [42] M. Kawamura, Y. Gohda, and S. Tsuneyuki, Improved tetrahedron method for the Brillouin-zone integration applicable to response functions, *Phys. Rev. B* **89**, 094515 (2014).
- [43] T. Nomoto, M. Kawamura, T. Koretsune, R. Arita, T. Machida, T. Hanaguri, M. Kriener, Y. Taguchi, and Y. Tokura, Microscopic characterization of the superconducting gap function in $\text{Sn}_{1-x}\text{In}_x\text{Te}$, *Phys. Rev. B* **101**, 014505 (2020).
- [44] M. Simonato, M. I. Katsnelson, and M. Rösner, Revised Tolmachev-Morel-Anderson pseudopotential for layered conventional superconductors with nonlocal Coulomb interaction, *Phys. Rev. B* **108**, 064513 (2023).
- [45] R. Akashi, K. Nakamura, R. Arita, and M. Imada, High-temperature superconductivity in layered nitrides $\beta\text{-Li}_x\text{MNCI}$ ($M = \text{Ti, Zr, Hf}$): Insights from density functional theory for superconductors, *Phys. Rev. B* **86**, 054513 (2012).
- [46] See Supplemental Material at [URL will be inserted by publisher] for relaxed crystal structure parameters, superconducting gap evolution with temperature, and other supporting data of this study.
- [47] M. Wierzbowska, S. de Gironcoli, and P. Giannozzi, Origins of low- and high-pressure discontinuities of T_c in niobium (2006), [arXiv:cond-mat/0504077](https://arxiv.org/abs/cond-mat/0504077).
- [48] F. Essenberg, A. Sanna, A. Linscheid, F. Tandetzky, G. Profeta, P. Cudazzo, and E. K. U. Gross, Superconducting pairing mediated by spin fluctuations from first principles, *Phys. Rev. B* **90**, 214504 (2014).
- [49] K. Tsutsumi, Y. Hizume, M. Kawamura, R. Akashi, and S. Tsuneyuki, Effect of spin fluctuations on superconductivity in V and Nb: A first-principles study, *Phys. Rev. B* **102**, 214515 (2020).
- [50] N. F. Berk and J. R. Schrieffer, Effect of ferromagnetic spin correlations on superconductivity, *Phys. Rev. Lett.* **17**, 433 (1966).
- [51] P. Tsuppayakorn-ae, T. Bovornratanaraks, R. Ahuja, W. Luo, and K. Kotmool, Hydrogen-induced phase stability and phonon mediated-superconductivity in two-dimensional van der Waals Ti_2C MXene monolayer, *Phys. Chem. Chem. Phys.* **25**, 2227 (2023).
- [52] S. Grimme, Semiempirical GGA-type density functional constructed with a long-range dispersion correction, *J. Comput. Chem.* **27**, 1787 (2006).
- [53] S. Grimme, J. Antony, S. Ehrlich, and H. Krieg, A consistent and accurate *ab initio* parametrization of density functional dispersion correction (DFT-D) for the 94 elements H-Pu, *J. Chem. Phys.* **132**, 154104 (2010).
- [54] A. D. Becke and E. R. Johnson, A simple effective potential for exchange, *J. Chem. Phys.* **124**, 221101 (2006).